








# Spontaneous ferroelectric order in lead-free relaxor $\text{Na}_{1/2}\text{Bi}_{1/2}\text{TiO}_3$ -based composites

Lalitha K. V. <sup>1,\*</sup> Manuel Hinterstein <sup>2</sup> Kai-Yang Lee <sup>2</sup> Tiannan Yang <sup>3</sup> Long-Qing Chen <sup>3</sup> Pedro B. Groszewicz,<sup>4</sup> Jurij Koruza <sup>1</sup> and Jürgen Rödel <sup>1</sup>

<sup>1</sup>Department of Materials and Earth Sciences, Technical University of Darmstadt, Darmstadt, Germany

<sup>2</sup>Institute for Applied Materials, Karlsruhe Institute of Technology, Karlsruhe, Germany

<sup>3</sup>Materials Research Institute and Department of Materials Science and Engineering, The Pennsylvania State University, University Park, Pennsylvania, USA

<sup>4</sup>Institute of Physical Chemistry, Technical University of Darmstadt, Darmstadt, Germany



(Received 6 September 2019; revised manuscript received 28 March 2020; accepted 30 March 2020; published 15 May 2020)

Short-range ordered polar nanoregions are key to the giant electromechanical properties exhibited by relaxor ferroelectrics. Stabilization of the long-range ferroelectric order in relaxor systems has typically been achieved by applying external fields. In this work, spontaneous (zero-field) ferroelectric order is demonstrated in the composites constituting of nonergodic relaxor matrix phase  $0.91\text{Na}_{1/2}\text{Bi}_{1/2}\text{TiO}_3$ - $0.09\text{BaTiO}_3$  with ZnO inclusions. Direct structural evidence is provided for the long-range ferroelectric order in the composites using *in situ* electric-field-dependent synchrotron investigations and  $^{23}\text{Na}$  nuclear magnetic resonance spectroscopy. Thermodynamic analysis incorporating microelasticity reveals the role of spatial residual stress in stabilizing the ferroelectric order. The work provides a direct correlation between the stabilized ferroelectric order and enhanced thermal stability, which can be utilized to guide the design of spontaneous long-range order in other relaxor systems.

DOI: [10.1103/PhysRevB.101.174108](https://doi.org/10.1103/PhysRevB.101.174108)

## I. INTRODUCTION

Relaxor ferroelectrics are distinct from normal ferroelectrics and can be differentiated based on the diffuse nature of the phase transformations. Unlike conventional ferroelectrics, the real part of permittivity in relaxors exhibit a broad peak as a function of temperature with strong frequency dispersion [1,2]. Relaxors, characterized by site and charge disorder associated with local polar heterogeneities, find applications as electromechanical actuators that exploit the giant strains exhibited by these systems, often resulting from phase transformations [3–7]. These transformations commonly take place upon application of an external stimulus, e.g., temperature, stress or electric field [4,8–11]. Although the majority of prior research focuses on the phase transformations that result in colossal strains in relaxor systems and related correlation to the structure and microstructure [12,13], relatively little attention has been devoted to understanding the spontaneous ferroelectric order in these systems. Some relaxors, upon cooling, spontaneously (without any external stimuli) transform into a ferroelectric state [14,15]. Spontaneous ferroelectric order that develops in the absence of an external stimulus is rare in relaxor systems [15,16] except the case of composition-induced development of ferroelectric order [17–20]. The stabilization of ferroelectric order in relaxor materials is often beneficial, since it enhances the critical phase transformation temperatures, thus increasing the thermal sta-

bility of the electromechanical properties and consequently the material's operational range of temperature [21]. In the case of *B*-site disordered  $\text{Pb}(\text{Sc}_{1/2}\text{Ta}_{1/2})\text{O}_3$ , which exhibits a spontaneous ferroelectric order,  $T_m$  (temperature at which the permittivity is maximum) shifts from  $-20$  to  $15^\circ\text{C}$  [14]. In the case of ordered  $\text{Pb}(\text{Sc}_{1/2}\text{Nb}_{1/2})\text{O}_3$ , the rhombohedral  $\rightarrow$  cubic phase transformation temperature increases by  $40^\circ\text{C}$  [15]. In the former, the ferroelectric order develops due to the ordering of the *B*-site cations, while in the latter, it is proposed that the presence of Pb vacancies limits the occurrence of ferroelectric order. In recent years, increase in the ferroelectric  $\rightarrow$  relaxor (FE  $\rightarrow$  RE) transformation temperature ( $T_{\text{F-R}}$ ) is reported for  $(1-x)\text{Na}_{1/2}\text{Bi}_{1/2}\text{TiO}_3$ - $x\text{BaTiO}_3$  (denoted as  $\text{NBT}_z\text{BT}$ ;  $z = 100x$ ) based materials and attributed to the stabilization of ferroelectric order [22–25].  $\text{NBT}_z\text{BT}$  exhibits a morphotropic phase boundary (MPB) between 5 and 12 mole % BT [20,26–28]. The most widely investigated compositional range is between 5 and 7 mole % BT, which is identified to be a core-MPB composition [29–31] and typically exhibits pseudocubic x-ray diffraction profiles [31], while the off-MPB compositions exhibit noncubic (rhombohedral/tetragonal) distortions [30]. Irrespective of the difference in the structural/microstructural features, the MPB composition range is established to exhibit nonergodic relaxor features [20,32]. The present work reports the development of spontaneous ferroelectric order in the composites of  $0.91\text{Na}_{1/2}\text{Bi}_{1/2}\text{TiO}_3$ - $0.09\text{BaTiO}_3$  ( $\text{NBT9BT}$ ) containing ZnO inclusions. These composites do not reveal a phase transformation upon application of electric field, while the nonergodic relaxor  $\text{NBT9BT}$  undergoes an irreversible transformation to

\*Corresponding author: [venkataraman@ceramics.tu-darmstadt.de](mailto:venkataraman@ceramics.tu-darmstadt.de)

the ferroelectric (RE→FE) state upon application of electric field or stress [10,31]. Although prior reports claim a stabilization of ferroelectric order [23,25], no direct structural evidence has been provided. This work presents a comparative structural investigation using *in situ* field-dependent synchrotron experiments and  $^{23}\text{Na}$  nuclear magnetic resonance spectroscopy ( $^{23}\text{Na}$  NMR) that clearly establishes the ferroelectric state of the composites. These observations also corroborate the electrical characterization and the absence of frequency dispersion in the permittivity response, typical for relaxor ferroelectrics. Thermodynamic analysis and microelasticity theory are employed to determine the threshold of residual stresses for inducing ferroelectric order in these material systems. The key findings of this work include (a) first direct structural evidence confirming spontaneous ferroelectric order in NBT9BT composites, (b) magnitude and scope of residual stresses in stabilizing ferroelectric order, and (c) demonstrated increase in the thermal depolarization temperature up to 180 °C, overcoming a long-withstanding problem of low thermal depolarization temperature of  $\text{Na}_{1/2}\text{Bi}_{1/2}\text{TiO}_3$ -based materials.

## II. METHODS

### A. Experimental

The composites constitute of NBT9BT matrix phase with  $y$  mole ratio of ZnO inclusions (NBT9BT: $y\text{ZnO}$ ;  $y = 0, 0.1, 0.2$  mole ratio, corresponding to 0, 3.87 and 7.45 vol.%, respectively). Stoichiometric amounts of  $\text{Bi}_2\text{O}_3$ ,  $\text{BaCO}_3$ ,  $\text{Na}_2\text{CO}_3$ , and  $\text{TiO}_2$  (Alfa Aesar) were milled for 24 h in ethanol at 250 rpm in a planetary ball mill. The powders were calcined at 900 °C for 3 h and remilled for 24 h in ethanol at 250 rpm. The dried powders were sieved and annealed at 1100 °C for 3 h. The coarsened NBT9BT powders were sieved and milled together with ZnO (25 nm, PlasmaChem GmbH) to form NBT9BT: $y\text{ZnO}$  composites. The composites were sintered at 1000–1050 °C for 1 h at a heating rate of 9 K/min. For reference, NBT9BT disks were sintered using noncoarsened powders at 1150 °C for 3 h with a heating rate of 5 K/min. The sintered samples were ground to remove material from the surface and electroded with silver paste, which was burned-in at 400 °C. Permittivity as a function of frequency and temperature was measured using an impedance analyzer (4192A LF, Hewlett-Packard, respectively). Polarization and strain hysteresis were obtained using a Sawyer-Tower circuit and an optical displacement sensor. *In situ* synchrotron diffraction experiments were performed on virgin (unpoled) samples ( $1 \times 1 \times 5 \text{ mm}^3$ ), electroded with sputtered platinum, at the P02.1 beamline [33,34] at the *Deutsches Elektronensynchrotron* (DESY) in Hamburg, Germany. The wavelength used was 0.20715 Å. The diffraction data was obtained upon application of electric field of amplitude 5.5 kV/mm (data measured in 41 steps up to 5.5 kV/mm with a collection of time of 30 s per step). The diffraction images were divided into 18 azimuthal sectors ( $\psi$ ) of 5° widths, with the azimuthal sector most closely oriented to the direction of applied electric field defined as  $\psi = 0^\circ$ . Refinements were performed using MAUD to extract the structural parameters including a texture model [35]. The  $^{23}\text{Na}$  NMR experiments

were performed on sintered, unpoled pellets and the details of the experimentation are reported elsewhere [36].

All the structural and electrical measurements were made from samples sintered from the same powder batches. Since the diffraction measurements need special geometries, bar shaped samples ( $1 \times 1 \times 5 \text{ mm}^3$ ) were cut out from sintered disks. The permittivity was measured from sintered disks, which were poled prior to the measurement. The strain data ( $S_{\text{optical}}$ ) is obtained from the same bar-shaped sample used in the diffraction measurement, with the same frequency used in the diffraction measurement (0.2 mHz). Since the samples used for synchrotron diffraction had already experienced higher electric fields, the samples were annealed at 400 °C for 30 min prior to the hysteresis measurements in the virgin state.

### B. Thermodynamic analysis and microelasticity theory

The residual stress is calculated by employing microelasticity theory. The mechanical equilibrium equation of the system is established as

$$\nabla \cdot \sigma = 0, \quad \sigma = \mathbf{c}(\epsilon - \epsilon_0). \quad (1)$$

Here  $\sigma$  is the stress field,  $\epsilon$  is the strain field, and  $\mathbf{c}$  is the elastic stiffness tensor of the material, taken as  $c_{11} = 181 \text{ GPa}$ ,  $c_{12} = 105 \text{ GPa}$ ,  $c_{44} = 79 \text{ GPa}$  for the NBT9BT phase [37] and  $c_{11} = 210 \text{ GPa}$ ,  $c_{12} = 121 \text{ GPa}$ ,  $c_{44} = 43 \text{ GPa}$  for the ZnO phase [38], respectively.  $\epsilon^0$  is the lattice mismatch strain from thermal expansion mismatch between the two phases, given by  $\epsilon^0 = 0$  for the NBT9BT phase and  $\epsilon^0 = (298\text{K} - T_{\text{sinter}})(\alpha^{\text{ZnO}} - \alpha^{\text{NBT9BT}}) = 0.0037$  for the ZnO phase, respectively.  $T_{\text{sinter}} = 1285 \text{ K}$  is the sintering temperature,  $\alpha^{\text{NBT9BT}} = 10.5 \times 10^{-6} \text{ K}^{-1}$  is the thermal expansion coefficient of NBT9BT [39] and  $\alpha^{\text{ZnO}} = 6.7 \times 10^{-6} \text{ K}^{-1}$  is the thermal expansion coefficient of ZnO, taken as the weighted average of the value along the crystallographic  $c$  axis,  $4.7 \times 10^{-6} \text{ K}^{-1}$ , and that along the  $a$  axes,  $7.7 \times 10^{-6} \text{ K}^{-1}$ , of a wurzite crystal structure [40]. The system consists of two spherical ZnO particles embedded in a NBT9BT matrix following the given phase fractions. A stress-free boundary condition is adopted. Eq. (1) is then solved using a Fourier-spectral iterative-perturbation method [41].

The free energy density of a ferroelectric NBT9BT domain with polarization  $\mathbf{P}$  under an electric field  $\mathbf{E}$  and a stress field  $\sigma$  is calculated as

$$f = f_{\text{Landau}}(\mathbf{P}) - P_i E_i - \sigma_{ij} Q_{ijkl} P_k P_l, \quad (2)$$

where  $\mathbf{Q}$  is the electrostrictive tensor.  $f_{\text{Landau}}$  is the Landau free energy density of the ferroelectric domain, written as a sixth-order polynomial of  $\mathbf{P}$ , i.e.,

$$\begin{aligned} f_{\text{Landau}}(\mathbf{P}) = & a_1(P_1^2 + P_2^2 + P_3^2) + a_{11}(P_1^4 + P_2^4 + P_3^4) \\ & + a_{12}(P_1^2 P_2^2 + P_1^2 P_3^2 + P_2^2 P_3^2) \\ & + a_{111}(P_1^6 + P_2^6 + P_3^6) \\ & + a_{112}(P_1^4 P_2^2 + P_1^4 P_3^2 + P_2^4 P_1^2 + P_2^4 P_3^2 \\ & + P_3^4 P_1^2 + P_3^4 P_2^2) + a_{123} P_1^2 P_2^2 P_3^2, \end{aligned} \quad (3)$$

where  $a_1$ ,  $a_{11}$ ,  $a_{12}$ ,  $a_{111}$ ,  $a_{112}$ , and  $a_{123}$  are the Landau coefficients of NBT9BT. The Landau coefficients and electrostrictive coefficients are obtained through fitting

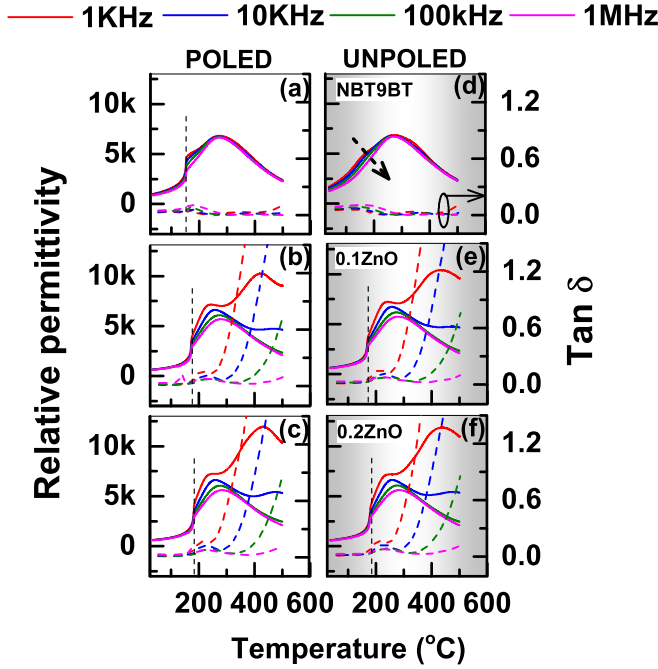


FIG. 1. Temperature- and frequency- dependent permittivity (heating cycle) of the composites in comparison to NBT9BT. The dashed arrow indicates the increasing order of frequency of the measurement. The dashed vertical lines denote  $T_{F-R}$ .

the temperature-dependent permittivity, the spontaneous polarization, the dielectric constant, the composition at the cubic-to-tetragonal transformation, and the lattice parameters of NBT<sub>z</sub>BT to previous experiments [42–44,27,10]. At room temperature,  $a_1 = -3.02 \times 10^7 \text{ JmC}^{-2}$ ,  $a_{11} = 8.01 \times 10^7 \text{ Jm}^5\text{C}^{-4}$ ,  $a_{12} = 3.22 \times 10^8 \text{ Jm}^5\text{C}^{-4}$ ,  $a_{111} = 4.52 \times 10^8 \text{ Jm}^9\text{C}^{-6}$ ,  $a_{112} = 7.79 \times 10^9 \text{ Jm}^9\text{C}^{-6}$ ,  $a_{123} = -4.60 \times 10^{10} \text{ Jm}^9\text{C}^{-6}$ ,  $Q_{11} = 0.133 \text{ m}^4\text{C}^{-2}$ ,  $Q_{12} = -0.027 \text{ m}^4\text{C}^{-2}$ , and  $Q_{44} = 0.072 \text{ m}^4\text{C}^{-2}$  for NBT9BT.

### III. RESULTS AND DISCUSSION

#### A. Dielectric and ferroelectric response

Verification of phase purity in accordance with the constituent phases, microstructure and grain size are provided in Fig. S1 [57]. Upon heating, the electric field-induced ferroelectric state of NBT9BT transforms to an ergodic relaxor state at  $T_{F-R}$ , which can be clearly observed from the first anomaly in the poled permittivity, indicated by a dashed vertical line [Fig 1(a)]. In comparison, the unpoled state of NBT9BT does not feature this transformation and exhibits a frequency dispersion in the permittivity response, typical of relaxor ferroelectrics [Fig. 1(b)]. Contrasting this behavior of NBT9BT to the composites, a strikingly different trend is observed. There is no frequency dispersion observed in the unpoled state of the composites below  $T_{F-R}$  [Figs. 1(e) and 1(f)]. In fact, the poled and unpoled permittivity responses are identical for the composites [Figs. 1(b), 1(c), 1(e), and 1(f)].

The nonergodic relaxor NBT9BT composition exhibits a large increase in strain ( $S_{pol}$ ) upon application of electric field in the unpoled state (Fig. S2b) [57]. The large increase in strain in nonergodic relaxors is attributed to the field-induced

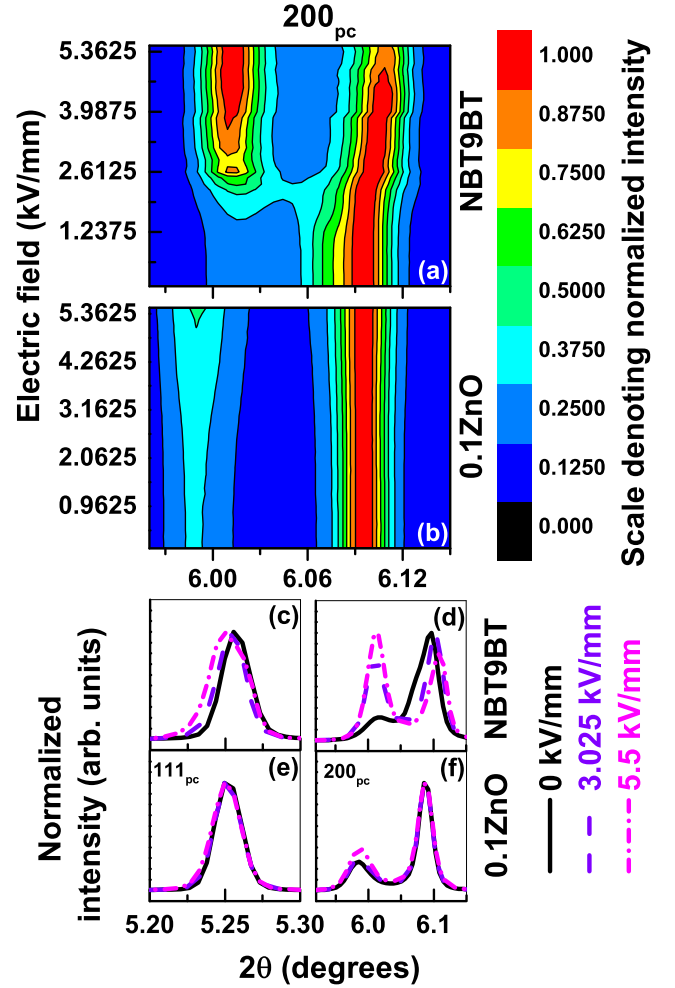


FIG. 2. *In situ* synchrotron investigations on NBT9BT and composite with 0.1 mole ratio of ZnO. (a), (b) depicts the evolution of  $200_{pc}$  reflection upon application of electric field from the unpoled state of the material. (c)–(f) compares the  $hkl_{pc}$  reflections at critical fields for  $\psi = 0$ .

RE→FE transformation [31,45–47]. The contributions to  $S_{pol}$  are twofold: strain due to the field-induced phase transformation and domain switching in the induced ferroelectric state. The very fact that  $S_{pol}$  is considerably lower for the composites (0.14%) compared to NBT9BT (0.40%) indicates that either both the contributions are lower for the composites or the strain due to the phase transformation is nonexistent. The absence of frequency dispersion in the permittivity response for the composites implies that the composites are ferroelectric. Therefore, there should be no field-induced phase transformation upon application of electric field for the composites, as opposed to NBT9BT. This is further addressed by *in situ* field-dependent diffraction investigations (Fig. 2), which offer the possibility to simultaneously track the field-induced phase transformation and lattice strain response.

#### B. Phase transformation from local and global structural investigations

The profile evolution of  $200_{pc}$  for NBT9BT and composite NBT9BT:0.1ZnO is depicted in Figs. 2(a) and 2(b). The

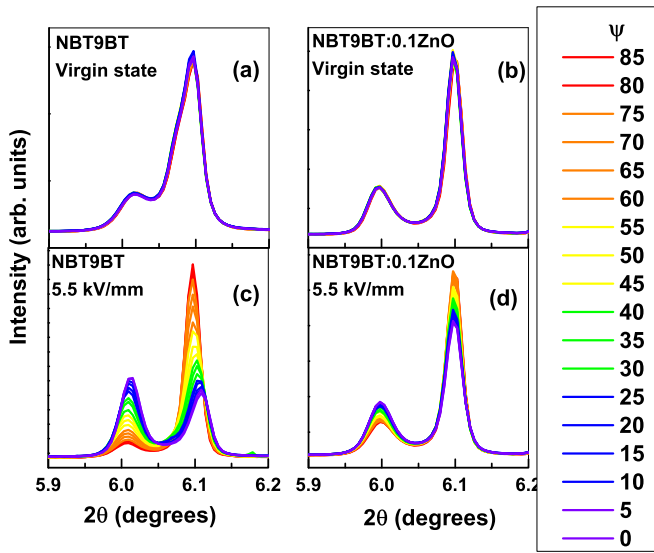


FIG. 3. Azimuthal ( $\psi$ ) dependence of the  $200_{pc}$  diffraction profile of NBT9BT and composite NBT9BT:0.1ZnO at (a), (b) 0 kV/mm (virgin) and (c), (d) 5.5 kV/mm.

subscript pc indicates pseudocubic indexing. In the case of NBT9BT, there is a clear change in the intensity and position of the  $200_{pc}$  reflection with increasing field amplitude, confirming a RE $\rightarrow$ FE transformation [Figs. 2(a), 2(c), and 2(d)]. The  $111_{pc}$  and  $200_{pc}$  reflections also exhibit broadening due to the field-induced phase transformation [Figs. 2(c) 2(d)]. In contrast, there is no change in the intensity and negligible reflection shifts for the composite [Figs. 2(b), 2(e), and 2(f)]. The azimuthal dependence of the  $200_{pc}$  upon application of electric field for select orientation is provided as contour plots in Fig. S3 [57]. Although the electric field (5.5 kV/mm) is sufficient to obtain saturated hysteresis (Fig. S2) [57], the absence of strong changes in intensity for the composite NBT9BT:0.1ZnO is intriguing. Hence, the azimuthal dependence of the  $200_{pc}$  upon application of electric field is plotted in Fig. 3 to track the development of texture. A careful look at the data did indicate a texture for the composite NBT9BT:0.1ZnO, nevertheless weaker than that observed for NBT9BT. A clear indication of texture is the change of the peak intensities as a function of azimuth (orientation of grain normal with respect to the direction of the electric field). In Fig. 3, the legend from 0 to 85 denotes the different azimuthal orientations. Note that in the unpoled state, both NBT9BT and the composite NBT9BT:0.1ZnO demonstrate no azimuthal dependence. However, at 5.5 kV/mm, both samples exhibit intensity changes, indicative of texturing, with the strongest texture observed for NBT9BT. Since texturing directly relates to the domain switching events, the weak texturing in the composite NBT9BT:0.1ZnO is indicative of electromechanical hardening [48].

NBT9BT undergoes a field-induced  $P4bm + R3c \rightarrow P4mm$  phase transformation. X-ray diffraction data is insensitive to superlattice reflections from  $P4bm$ . Therefore, the structure was refined using  $P4mm + R3c$  phase [31,49] and a texture model to account for the field-induced domain switching that results in texture. The strain, calculated with

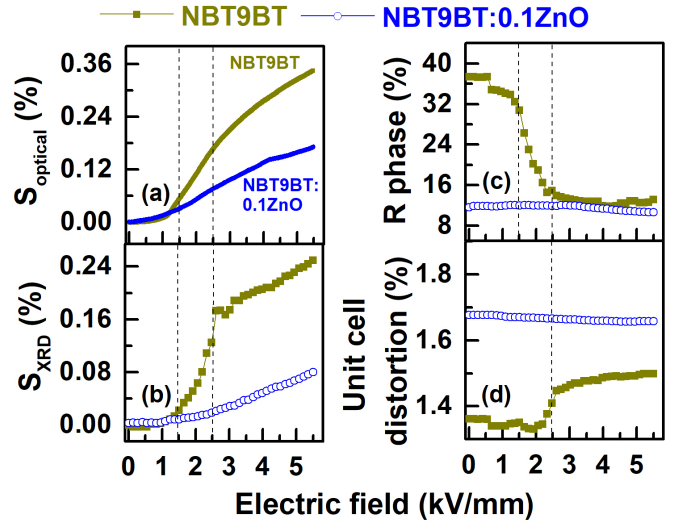


FIG. 4. (a) Macroscopic strain measured from the bar-shaped synchrotron samples using an optical displacement sensor. Strain (b), rhombohedral phase fraction (c) and tetragonal unit cell distortion (d) evaluated from the *in situ* electric field-dependent synchrotron data. The dashed lines denote the inflection points corresponding to the start and end of the field-induced phase transformation from the relaxor to the ferroelectric state.  $S_{optical}$  is obtained from the same sample used in the synchrotron measurement at 0.2 mHz. Since the samples used in the synchrotron measurements had already experienced high electric fields, the samples were annealed before performing the strain-field hysteresis.

“Strain, Texture, and Rietveld Analysis for Piezoceramics” (STRAP) [50] and the phase fraction extracted from the refined dataset are plotted in Fig. 4. Representative fits of the data are plotted in Fig. S4 [57]. NBT9BT:0.1ZnO exhibits a 68% decrease in field-induced macroscopic strain (evaluated from the synchrotron dataset) in comparison to NBT9BT [Fig. 4(b)]; this decrease closely corresponds to the 50% decrease, established from the macroscopically measured strain hysteresis [Fig. 4(a)]. The discrepancy in the absolute strain values from macroscopic and diffraction measurements can be due to the difference in the cyclic and step-wise measurements, respectively, which has also been observed in other studies employing *in situ* diffraction [51]. During the field-induced phase transformation, the rhombohedral phase with a low unit cell distortion is transformed to the tetragonal phase with a larger unit cell distortion. The grains subjected to this transformation have a preferred orientation that is favorable for tetragonal symmetry. The resulting electric-field-induced strain therefore has contributions from the phase transformation and reorientation of the non- $180^\circ$  domains. Lattice strain does not play a significant role for both systems. The electric-field-dependent tetragonal unit cell distortions are depicted in Fig. 4(d). In the unpoled state, NBT9BT has a lower tetragonal unit cell distortion (1.36%) as compared to composite NBT9BT:0.1ZnO (1.68%) (Table I). Upon application of electric field, the unit cell distortion in NBT9BT increases from 1.36% to 1.5%. In comparison, the tetragonal unit cell distortion of poled NBT7BT was reported to be 1.3% [31]. This increase in strain of about 0.14% for NBT9BT coincides with the irreversible strain observed macroscopically. The



TABLE I. Summary of refined structural parameters in the poled and unpoled state for NBT9BT and composite NBT9BT:0.1ZnO.  $a_T$ ,  $c_T$ ,  $a_H$ , and  $c_H$  are the tetragonal and rhombohedral (hexagonal setting) lattice parameters,  $V_T$  and  $V_{R,pc}$  the tetragonal and rhombohedral pseudocubic unit cell volumes,  $\eta_T$  and  $\eta_R$  the tetragonal and rhombohedral unit cell distortions and  $F_T$ , the tetragonal phase fraction.

	NBT9BT		NBT9BT:0.1ZnO	
	Unpoled	Max. field	Unpoled	Max. field
$a_T$ (Å)	3.89214(3)	3.89075(2)	3.89127(2)	3.89150(2)
$c_T$ (Å)	3.94510(7)	3.94905(4)	3.95653(3)	3.95601(4)
$V_T$ (Å <sup>3</sup> )	59.763(4)	59.780(3)	59.9096(9)	59.9088(10)
$\eta_T$ (%)	1.361(3)	1.499(2)	1.677(2)	1.658(2)
$F_T$ (%)	63(1)	87(1)	88(2)	89(2)
$a_H$ (Å)	5.52374(7)	5.5176(3)	5.52899(16)	5.5292(2)
$c_H$ (Å)	6.7739(3)	6.7883(3)	6.7817(5)	6.7793(6)
$V_{R,pc}$ (Å <sup>3</sup> )	59.664(4)	59.659(5)	59.847(4)	59.830(5)
$\eta_R$ (%)	0.129(4)	0.453(6)	0.149(11)	0.110(13)

composite NBT9BT:0.1ZnO exhibits a field-dependent strain variation of only 0.05%, which is three times lower than that of NBT9BT. Note that the total strain established from the strain-field hysteresis [Fig. 4(a)] and STRAP [Fig. 4(b)] is also three times lower for the composite NBT9BT:0.1ZnO in comparison to NBT9BT. The rhombohedral phase fraction [Fig. 4(c)] decreases for NBT9BT as expected [31]. The composite NBT9BT:0.1ZnO exhibits negligible changes in the phase fraction, which confirms the absence of field-induced phase transformation. The lower field-induced strain and reduced rhombohedral phase fraction further confirm the ferroelectric state of the composites.

<sup>23</sup>Na NMR has been previously used to quantify the cubic and noncubic phase fractions in the poled and unpoled states of relaxor NBT<sub>z</sub>BT [36]. As demonstrated in Fig. 5, unpoled NBT9BT exhibits a cubic phase fraction of  $18 \pm 2.5\%$ , while this amount is reduced to  $5 \pm 2.5\%$  for the unpoled composite NBT9BT:0.1ZnO. The latter closely matches to the cubic phase fraction in the poled state of NBT<sub>z</sub>BT, which corroborates the absence of relaxor features in the unpoled composites [36].

### C. Thermodynamic calculations incorporating microelasticity theory

Stabilization of ferroelectric order has been reported previously using external stimuli, namely electric field or stress [10,31]. Recently, electric depoling was also shown to retain the ferroelectric state in NBT7BT [49]. The present work reports a ferroelectric state that develops spontaneously in the absence of external stimuli. Given that cation ordering can also result in a ferroelectric order [14], no such effects have been reported for NBT<sub>z</sub>BT [52]. Note that prior work on the composites also indicated a stabilization of the ferroelectric order that led to the enhancement of  $T_{F-R}$  in NBT6BT:yZnO [23]. The results were explained on the basis of a residual-stress-induced stabilization of the ferroelectric order. Herein, Landau theory combined with microelasticity theory is used to explain the role of residual stresses in the composites. Fig-

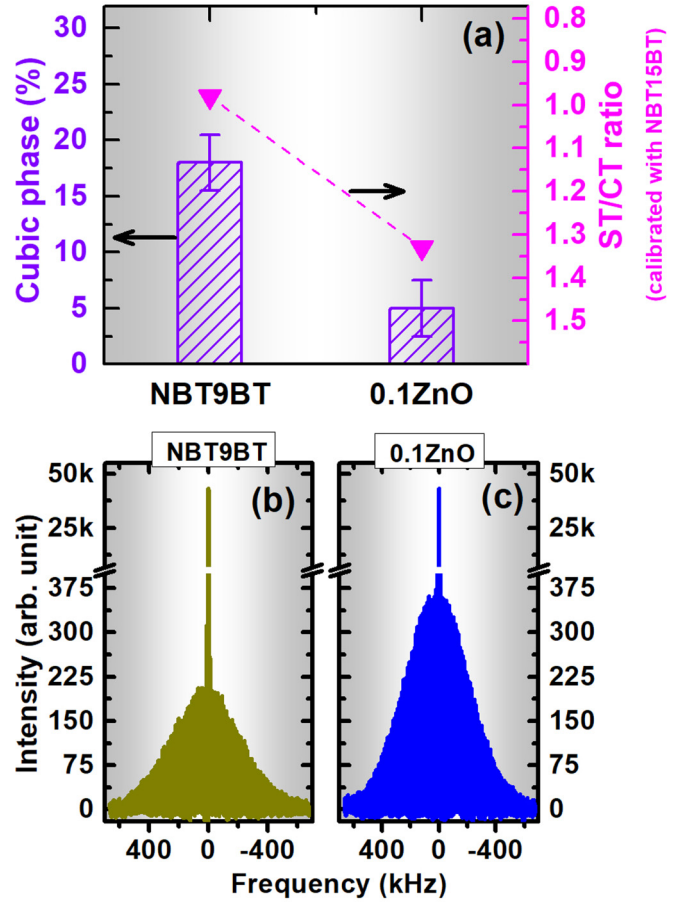


FIG. 5. (a) Cubic phase fraction and the intensity ratio between the satellite (ST) and central (CT) transitions evaluated from the <sup>23</sup>Na NMR spectra for unpoled samples. The central and satellite transitions are depicted in the figures below (b), (c).

ures 5(a) and 5(b) provide the polarization-dependent free energy function of the ferroelectric tetragonal and rhombohedral phases in NBT9BT and the composite NBT9BT:0.1ZnO. According to our experiment [Fig. 4(a)], a transformation from the relaxor state to the ferroelectric state occurs in NBT9BT upon applying an electric field of  $E = 3$  kV/mm. The free energy of the ferroelectric tetragonal phase at the field-induced transformation is calculated as  $f_0 = -2.76$  MJ/m<sup>3</sup> following the energy minimum of Eq. (2) with  $E = 3$  kV/mm and  $\sigma = 0$ . Alternatively, the free energy of the tetragonal phase at the field-induced transformation can also be approximated as  $f_0 \approx f'_0 - P_s E$ , where  $f'_0 = -1.77$  MJ/m<sup>3</sup> is the free energy of the ferroelectric tetragonal phase (i.e., the minimum of the free energy function achieved at  $P = 0.32$  C/m<sup>2</sup>) under zero field and  $P_s = 0.32$  C/m<sup>2</sup> is the spontaneous polarization. With  $E = 3$  kV/mm, we obtain a similar value of  $f_0 \approx -2.73$  MJ/m<sup>3</sup>.  $f_0$  is taken as the critical free energy for the formation of the ferroelectric phase, i.e., the ferroelectric state will form if the local free energy density follows  $f \leq f_0$ . For NBT9BT under stress-free condition, the free energy of the ferroelectric tetragonal phase is calculated as  $-1.77$  MJ/m<sup>3</sup>, which is above the critical free energy of the RE→FE transformation at  $f_0 = -2.76$  MJ/m<sup>3</sup> [Fig. 5(c)]. Hence, for unpoled NBT9BT, the relaxor phase is more stable than the

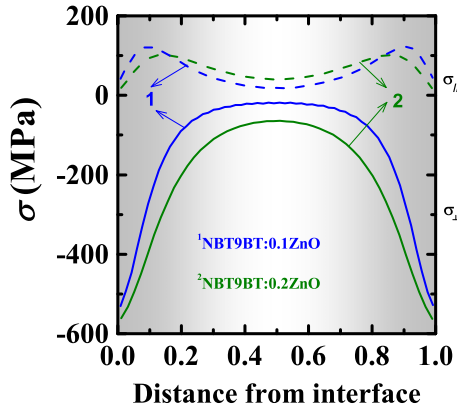


FIG. 6. Stress components (dashed curves)  $\sigma_{\parallel}$  parallel to the matrix/inclusion interface and (solid curves)  $\sigma_{\perp}$  perpendicular to the matrix/inclusion interface as a function of distance from the interface, in the NBT9BT matrix of the NBT9BT:0.1ZnO and NBT9BT:0.2ZnO composites. The distance adopts a reduced unit, where 0 and 1 indicate the two NBT9BT/ZnO interfaces between the NBT9BT phase and two neighboring ZnO inclusions, respectively.

ferroelectric phase. In the case of NBT9BT:yZnO composites, the mismatch in the thermal expansion coefficient between NBT9BT and ZnO phases result in anisotropic residual stress in the NBT9BT phase near the NBT9BT/ZnO interface, with a tensile component ( $\sigma_{\parallel} > 0$ ) parallel to the NBT9BT/ZnO interface and a compressive component ( $\sigma_{\perp} < 0$ ) perpendicular to the interface (Fig. 6). Such residual stress favors a polarization direction parallel to the interface plane, with a much lower free energy than the stress-free case according to our calculations. For example, the free energy of the tetragonal ferroelectric phase at the NBT9BT/ZnO interface in the NBT9BT:0.1ZnO composite is estimated as  $-4.22 \text{ MJ/m}^3$  [Fig. 7(a)], which is lower than the critical energy for RE  $\rightarrow$  FE transformation at  $f_0 = -2.76 \text{ MJ/m}^3$ . A local ferroelectric phase is thus energetically stabilized. Similarly, the ferroelectric rhombohedral phase in the NBT9BT:0.1ZnO composite also features an increased stability compared to that of NBT9BT [Fig. 7(b)]. At this juncture, it is worth noting that the NBT6BT:yZnO composites did not exhibit a spontaneous RE  $\rightarrow$  FE transformation [23]. NBT6BT:yZnO composites demonstrate an increase in  $T_{F-R}$ , yet exhibited relaxor features in the unpoled state [23]. Recent work on quenching NBTzBT compositions also confirm this premise, wherein NBT6BT and NBT9BT quenched from sintering temperatures were reported to exhibit an increased  $T_{F-R}$ ; however, spontaneous transformation to the ferroelectric state was observed only for quenched NBT9BT, whereas quenched NBT6BT exhibited relaxor features [25]. As has been stated, NBT9BT is an off-MPB composition (as opposed to NBT6BT, which is a core-MPB composition), close to the phase boundary of composition induced relaxor-ferroelectric crossover [20,53]. Therefore, NBT9BT exhibits strong predisposition to transform into a ferroelectric state as opposed to NBT6BT and the residual stresses in the composite facilitate this transformation. This is also evident from the  $^{23}\text{Na}$  NMR experiments, wherein the cubic phase fraction is evaluated to be 23% for NBT6BT [23] as opposed to 18% for NBT9BT, indicating

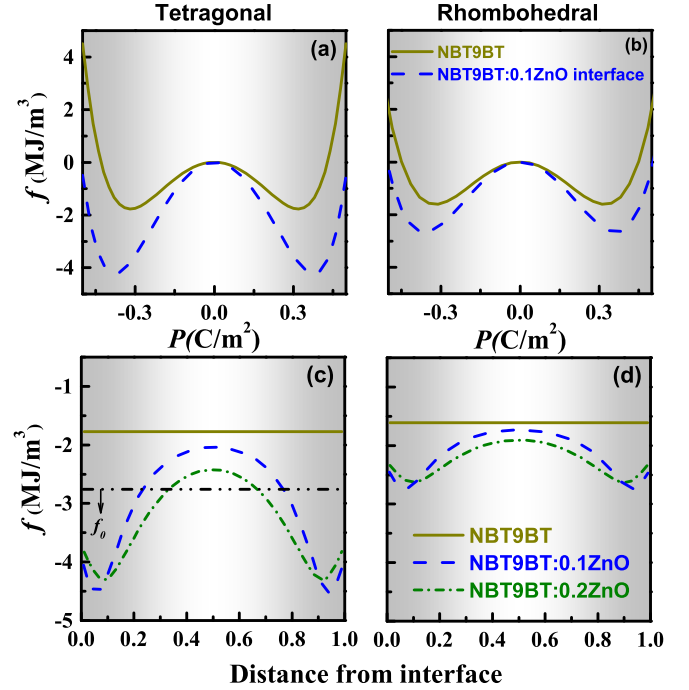


FIG. 7. Free energy density of NBT9BT and NBT9BT regions around the matrix/inclusion interface in the NBT9BT:0.1ZnO composite as a function of polarization for the (a) tetragonal and (b) rhombohedral phases. A more negative free energy density indicates a more stable phase. Free energy density of the (c) tetragonal and (d) rhombohedral phases as a function of distance from the matrix/inclusion interface. The dash-dotted line indicates the free energy ( $f_0$ ) required for NBT9BT to stabilize in the ferroelectric state.

more propensity for NBT9BT to spontaneously develop a ferroelectric order.

#### D. Role of residual stress in stabilizing the ferroelectric order

Considering the open structure of the perovskite lattice and the high processing temperatures, it is plausible that zinc ions from the ZnO inclusions diffuse into the matrix NBT9BT phase, thus leading to the development of ferroelectric order. Previously, diffraction investigations of the composite NBT6BT:0.3ZnO suggested changes in the unit cell volume and attributed this change to the stabilized ferroelectric order [54,55]. The changes in unit cell volume were concluded to result from diffusion of zinc into the matrix NBT6BT phase. Nevertheless, these investigations were made on powders obtained from crushing the composite pellet and, therefore, do not provide a description of the residual stress effects. In the case of NBT6BT, the rhombohedral unit cell distortion is as high as 0.8% under compressive stress loading [10]. Therefore, the increase in unit cell distortion need not necessarily result from chemical doping. Recently, selective diffusion of zinc into the matrix phase was reported for the composite NBT6BT:0.3ZnO using transmission electron microscopy-energy dispersive x-ray spectroscopy [56]. The strain fields evaluated at the interface were not conclusive on the role of residual stresses. Hence, from the arguments of thermodynamic equilibrium, it is clearly established that the residual

stresses (Fig. 6) are instrumental in stabilizing the ferroelectric order (Fig. 7), while at the same time, doping will also impact the phase equilibria. The spatially dependent free energy profile of the ferroelectric phase is depicted in Figs. 7(c) and 7(d). In comparison with the stress-free NBT9BT, the free energy is significantly decreased only in regions close to the NBT9BT/ZnO interface, while such an effect is much weaker in regions far away from the interface [Fig. 6(d)]. This is due to the fast decay of the residual stress with increasing distance away from the interface [23]. For example, in the NBT9BT:0.1ZnO composite, the residual compressive stress  $\sigma_{\perp}$  is  $< 20$  MPa for regions beyond 20% of the normalized distances from the interface (Fig. 6). At the matrix/inclusion interface, the residual compressive stress,  $\sigma_{\perp}$  is 489 MPa for NBT9BT:0.1ZnO (Fig. 6) and corresponds closely to the RE $\rightarrow$ FE transformation stress (325 MPa for NBT6BT) in a model experiment of far-field uniaxial compressive loading [10]. Prior analytical modeling of a single particle in an infinite isotropic matrix evaluated the residual radial compressive stress at the interface to be 388 MPa for NBT6BT:0.1ZnO [23]. In comparison to the previous study [23], the current model also accommodates for the distribution of inclusions in the matrix phase. The volume fractions of the ferroelectric phase stabilized by the residual stress are estimated as 7.2% and 11.1% for NBT9BT:0.1ZnO and NBT9BT:0.2ZnO composites, respectively. Note that prior work estimated the transformed volume to be 2.4% for NBT6BT:0.1ZnO [23]. In comparison, the change in the  $R3c$  phase fraction established from diffraction studies is 24% in the unpoled state between NBT9BT and the composite NBT9BT:0.1ZnO (Table I). The limited effect of stresses, as established from Landau formalism, in addition to the higher unit cell distortion for the composites as opposed to NBT9BT [Fig. 4(d)], points to the role of Zn diffusion in the matrix NBT9BT phase. Since prior reports claim that Zn diffusion [56] or substitution [24] can also stabilize a ferroelectric phase, it is likely that the ferroelectric seeds that are stabilized using stress or chemical modification, can act as new nucleation sites for the expanse of the ferroelectric domains. Note that both the residual stress and diffusion of zinc are likely to be colocated at the NBT9BT/ZnO interface and, therefore, it is not trivial to distinguish these effects.

As mentioned earlier, the development of spontaneous ferroelectric order in a relaxor is observed as a rare occurrence in B-site disordered lead-based relaxors systems [18].

Spontaneous ferroelectric order was previously shown to stem from the ordering of the B-site cations [14] and is proportional to the mismatch of size and charge of the cations. The present work facilitates an alternative approach by tailoring the microstructure to spontaneously develop or stabilize the ferroelectric order in relaxor ferroelectrics and is not limited by the nature of the inherent structural disorder present in the system. Apart from providing an extrinsic approach for tailoring the long-range polar order, this approach is beneficial in increasing the thermal stability and hardening of the electromechanical properties [48].

#### IV. CONCLUSIONS

In summary, direct structural evidence for the long-range polar order is demonstrated in relaxor NBT9BT composites with ZnO inclusions, by elucidating the field-induced phase transformation and lattice strain using *in situ* diffraction investigations. The relatively small cubic phase fraction established from NMR analysis and the absence of frequency dispersion in the temperature-dependent permittivity further substantiate the ferroelectric state of the composites. Thermodynamic analysis elucidates the role of the residual stresses in inducing a ferroelectric phase. The results demonstrate that the increase in the critical FE $\rightarrow$  RE transformation temperature is a consequence of the stabilization of the ferroelectric order, which need not necessarily result from cation ordering effects, as is the case with B-site disordered Pb-based relaxors. The outcome of this work is expected to steer development of relaxors with enhanced temperature stability of the electromechanical properties.

#### ACKNOWLEDGMENTS

L.K.V. acknowledges and thanks the Alexander von Humboldt Foundation and the Deutsche Forschungsgemeinschaft under Grant No. KO 5948/1-1 (Nr. 414311761) for financial support. M.H. acknowledges the Deutsche Forschungsgemeinschaft under Grant No. HI 1867/1-1. The efforts at Penn State were supported by the National Science Foundation (NSF) under Grant No. DMR-1744213. L.Q.C. acknowledges the Humboldt Research Award. J. K. acknowledges the Deutsche Forschungsgemeinschaft under Grant No. KO 5100/3-1 (Nr. 414073759). P.B.G. acknowledges the Deutsche Forschungsgemeinschaft under Grants No. BU 911/28-1 and No. 397608312.

- [1] M. E. Lines and A. M. Glass, *Principles and Applications of Ferroelectrics and Related Materials* (Clarendon Press, Oxford, 1979).
- [2] A. J. Moulson and J. M. Herbert, *Electroceramics: Materials, Properties, Applications* (Wiley, New York, 2003).
- [3] S.-E. Park and T. R. Shrout, *J. Appl. Phys.* **82**, 1804 (1997).
- [4] Z. Kutnjak, J. Petzelt, and R. Blinc, *Nature (London)* **441**, 956 (2006).
- [5] R. E. Cohen, *Nature (London)* **441**, 941 (2006).
- [6] H. Fu and R. E. Cohen, *Nature (London)* **403**, 281 (2000).
- [7] Z.-G. Ye, *MRS Bull.* **34**, 277 (2009).
- [8] E. A. McLaughlin, T. Liu, and C. S. Lynch, *Acta Mater.* **52**, 3849 (2004).
- [9] M. Davis, D. Damjanovic, and N. Setter, *Phys. Rev. B* **73**, 014115 (2006).
- [10] F. H. Schader, Z. Wang, M. Hinterstein, J. E. Daniels, and K. G. Webber, *Phys. Rev. B* **93**, 134111 (2016).
- [11] J. Glaum, Y. Heo, M. Acosta, P. Sharma, J. Seidel, and M. Hinterstein, *Phys. Rev. Mater.* **3**, 054406 (2019).
- [12] A. Kholkin, A. Morozovska, D. Kiselev, I. Bdikin, B. Rodriguez, P. Wu, A. Bokov, Z.-G. Ye, B. Dkhil, L.-Q. Chen, M. Kosec, and S. V. Kalinin, *Adv. Funct. Mater.* **21**, 1977 (2011).
- [13] F. Li, D. Lin, Z. Chen, Z. Cheng, J. Wang, C. Li, Z. Xu, Q. Huang, X. Liao, L.-Q. Chen, T. R. Shrout, and S. Zhang, *Nat. Mater.* **17**, 349 (2018).

- [14] N. Setter and L. E. Cross, *J. Appl. Phys.* **51**, 4356 (1980).
- [15] F. Chu, I. M. Reaney, and N. Setter, *J. Appl. Phys.* **77**, 1671 (1995).
- [16] F. Chu, I. M. Reaney, and N. Setter, *Ferroelectrics* **151**, 343 (1994).
- [17] X. Dai, Z. Xu, and D. Viehland, *Philos. Mag. B* **70**, 33 (1994).
- [18] I. W. Chen, *J. Phys. Chem. Solids* **61**, 197 (2000).
- [19] L. Mitoseriu, A. Stancu, C. Fedor, and P. M. Vilarinho, *J. Appl. Phys.* **94**, 1918 (2003).
- [20] C. Ma, H. Guo, S. P. Beckman, and X. Tan, *Phys. Rev. Lett.* **109**, 107602 (2012).
- [21] J. Koruza, A. J. Bell, T. Frömling, K. G. Webber, K. Wang, and J. Rödel, *J. Materiomics* **4**, 13 (2018).
- [22] J. Zhang, Z. Pan, F.-F. Guo, W.-C. Liu, H. Ning, Y. B. Chen, M.-H. Lu, B. Yang, J. Chen, S.-T. Zhang, X. Xing, J. Rödel, W. Cao, and Y.-F. Chen, *Nat. Commun.* **6**, 6615 (2015).
- [23] L. M. Riemer, Lalitha K. V., X. Jiang, N. Liu, C. Dietz, R. W. Stark, P. B. Groszewicz, G. Buntkowsky, J. Chen, S.-T. Zhang, J. Rödel, and J. Koruza, *Acta Mater.* **136**, 271 (2017).
- [24] L. Li, M. Zhu, K. Zhou, Q. Wei, M. Zheng, and Y. Hou, *J. Appl. Phys.* **122**, 204104 (2017).
- [25] Lalitha K.V., J. Koruza, and J. Rödel, *Appl. Phys. Lett.* **113**, 252902 (2018).
- [26] T. Takenaka, *Ferroelectrics* **230**, 87 (1999).
- [27] W. Jo, J. E. Daniels, J. L. Jones, X. Tan, P. A. Thomas, D. Damjanovic, and J. Rödel, *J. Appl. Phys.* **109**, 014110 (2011).
- [28] K.-Y. Lee, X. Shi, N. Kumar, M. Hoffman, M. Etter, S. Checchia, J. Winter, L. Lemos da Silva, D. Seifert, and M. Hinterstein, *Materials* **13**, 1054 (2020).
- [29] M. Guennou, M. Savinov, J. Drahoukoupil, H. Luo, and J. Hlinka, *Appl. Phys. A* **116**, 225 (2013).
- [30] W. Jo, S. Schaab, E. Sapper, L. A. Schmitt, H.-J. Kleebe, A. J. Bell, and J. Rödel, *J. Appl. Phys.* **110**, 074106 (2011).
- [31] M. Hinterstein, L. A. Schmitt, M. Hoelzel, W. Jo, J. Rödel, H.-J. Kleebe, and M. Hoffman, *Appl. Phys. Lett.* **106**, 222904 (2015).
- [32] R. Ranjan and A. Dviwedi, *Solid State Commun.* **135**, 394 (2005).
- [33] M. Herklotz, F. Scheiba, M. Hinterstein, K. Nikolowski, M. Knapp, A.-C. Dippel, L. Giebeler, J. Eckert, and H. Ehrenberg, *J. Appl. Crystallogr.* **46**, 1117 (2013).
- [34] A.-C. Dippel, H.-P. Liermann, J. T. Delitz, P. Walter, H. Schulte-Schrepping, O. H. Seeck, and H. Franz, *J. Synchrotron Radiat.* **22**, 675 (2015).
- [35] M. Hinterstein, M. Hoelzel, J. Rouquette, J. Haines, J. Glaum, H. Kungl, and M. Hoffman, *Acta Mater.* **94**, 319 (2015).
- [36] P. B. Groszewicz, H. Breitzke, R. Dittmer, E. Sapper, W. Jo, G. Buntkowsky, and J. Rödel, *Phys. Rev. B* **90**, 220104(R) (2014).
- [37] B. W. Lee, J.-H. Ko, X. Li, and H. Luo, *J. Korean Phys. Soc.* **66**, 1350 (2015).
- [38] T. B. Bateman, *J. Appl. Phys.* **33**, 3309 (1962).
- [39] U. Lewczuk-Jodłowiec, J. Suchanicz, D. Sitko, and K. Konieczny, *Phase Transit.* **90**, 818 (2017).
- [40] H. Ibach, *Phys. Status Solidi B* **33**, 257 (1969).
- [41] S. Y. Hu and L. Q. Chen, *Acta Mater.* **49**, 1879 (2001).
- [42] T. Takenaka, K. Maruyama, and K. Sakata, *Jpn. J. Appl. Phys.* **30**, 2236 (1991).
- [43] G. Picht, J. Töpfer, and E. Hennig, *J. Eur. Ceram. Soc.* **30**, 3445 (2010).
- [44] F. Cordero, F. Craciun, F. Trequattrini, E. Mercadelli, and C. Galassi, *Phys. Rev. B* **81**, 144124 (2010).
- [45] N. H. Khansur, M. Hinterstein, Z. Wang, C. Groh, W. Jo, and J. E. Daniels, *Appl. Phys. Lett.* **107**, 242902 (2015).
- [46] F. Craciun, C. Galassi, and R. Birjega, *J. Appl. Phys.* **112**, 124106 (2012).
- [47] J. E. Daniels, W. Jo, J. Rödel, and J. L. Jones, *Appl. Phys. Lett.* **95**, 032904 (2009).
- [48] Lalitha K. V., L. M. Riemer, J. Koruza, and J. Rödel, *Appl. Phys. Lett.* **111**, 022905 (2017).
- [49] A. Martin, N. H. Khansur, and K. G. Webber, *J. Eur. Ceram. Soc.* **38**, 4623 (2018).
- [50] M. Hinterstein, K.-Y. Lee, S. Esslinger, J. Glaum, A. J. Studer, M. Hoffman, and M. J. Hoffmann, *Phys. Rev. B* **99**, 174107 (2019).
- [51] A. Pramanick and J. L. Jones, *IEEE Trans. Ultrason. Ferroelectr. Freq. Control* **56**, 1546 (2009).
- [52] J. Kling, S. Hayn, L. A. Schmitt, M. Gröting, H.-J. Kleebe, and K. Albe, *J. Appl. Phys.* **107**, 114113 (2010).
- [53] C. Ma, X. Tan, E. Dul'kin, and M. Roth, *J. Appl. Phys.* **108**, 104105 (2010).
- [54] A. Mahajan, H. Zhang, J. Wu, E. V. Ramana, M. J. Reece, and H. Yan, *J. Phys. Chem. C* **121**, 5709 (2017).
- [55] W. Bai, P. Zheng, F. Wen, J. Zhang, D. Chen, J. Zhai, and Z. Ji, *Dalton Trans.* **46**, 15340 (2017).
- [56] Z. Fan, L. Zhou, T.-H. Kim, J. Zhang, S.-T. Zhang, and X. Tan, *Phys. Rev. Mater.* **3**, 024402 (2019).
- [57] See Supplemental Material at <http://link.aps.org/supplemental/10.1103/PhysRevB.101.174108> for description of the constituent phases, microstructure and grain size (Fig. S1), polarization and strain-field hysteresis in the virgin state (Fig. S2), azimuthal dependence of the diffraction profiles with electric field (Fig. S3), and representative Rietveld fits of the diffraction data (Fig. S4).